Dyes and Pigments 95 (2012) 23–32

Contents lists available at SciVerse ScienceDirect

Dyes and Pigments

journal homepage: www.elsevier.com/locate/dyepig

Electroluminescence from two new ruthenium(II) complexes as phosphorescent dopant: Positive effect of swallow-tail bipyridyl ligand

Ilker Oner [a], Cigdem Sahin [b], Canan Varlikli [a,*]

[a] Ege University, Solar Energy Institute, 35100 Bornova-Izmir, Turkey
[b] Chemistry Department, Arts & Science Faculty, Pamukkale University, Denizli, Turkey

ARTICLE INFO

Article history:
Received 8 December 2011
Received in revised form
20 February 2012
Accepted 28 February 2012
Available online 16 March 2012

Keywords:
Amphiphilic ruthenium (II) complex
Chiral alkyl chain
Swallow-tail alkyl chain
Organic light emitting diode
Orange-red
Electroluminescence

ABSTRACT

Two new orange-red emitting ruthenium complexes, [Ru(bpy)2(4,4′-bis(3-ethylheptyl)-2,2′-bipyridine)]$(PF_6)_2$ and [Ru(bpy)2(4-dihexylmethyl-4′-heptyl-2,2′-bipyridine)]$(PF_6)_2$ with branched alkyl side groups on the bipyridyl ligand have been synthesized and used as dopants in an organic light emitting device. The device that contains the complex containing the 4-dihexylmethyl-4′-heptyl-2,2′-bipyridine ligand 1.0 wt.% doped polymer blends of poly(vinylcarbazole) and 2-tert-butylphenyl-5-biphenyl-1,3,4-oxadiazol as the emitting layer reached to a luminous efficiency of 7 cd/A, and a maximum brightness of 3824 cd/m^2 with an electroluminescence spectral peak at 600 nm and Commission Internationale de L'Eclairage chromaticity coordinates of (0.57, 0.39). The swallow-tail alkyl substituent in this complex played a significant role in lowering the tendency to aggregate and presenting a better electroluminescence efficiency than that of the complex derived from the 4,4′-bis(3-ethylheptyl)-2,2′-bipyridine) ligand in a device.

1. Introduction

The efficiency of an organic light emitting diode (OLED) strongly depends on the choice of molecules and the design of device structure. Recently, considerable progress has been achieved with electrophosphorescent OLEDs that involve the transition metal complexes as emitters [1–3]. The presence of transition metals provides the advantages of controlling and tuning of photophysical, photochemical and redox properties of materials [4]. Among them Os, Pt and Ir complexes have been subject of many reports in the field of OLED technology [5–8] to obtain red, green and blue colors. However, the cost of a technology is the major factor that will affect its commercialization. In this aspect for a red color, Ru(II) complexes are alternatives of those precious noble metal complexes that provide advantages of being a transition metal complexes [9–11].

Generally, Ru(II) complexes have been used in light emitting electrochemical cells (LECs) both in solution and solid state [12–20]. Stabilities of these cells are generally very low and response times are rather long when compared with the organic EL devices. Recently, there has been much effort to use these complexes as dopants in a proper matrix to overcome these hindrances [21–27]. In principle, a molecular dispersion of Ru(II)complexes in a semiconductor material surpasses the problems associated with counter ion mobility, self-quenching and triplet–triplet annihilation that is derived from the strong interaction between the molecules.

In this study, two Ru(II) complexes that contain symmetric and asymmetric branched alkyl chains on their bipyridyl (bpy) ligands were synthesized and used as a dopant in a wide band gap PVK:PBD blend host. As is well-known from the literature, a doping strategy may increase the EL performance through energy transfer or direct charge trapping [26]. The presence of branched alkyl groups on the bpy ligand may increase the compatibility between the polymer and the complexes [23,28]. The device that contains the complex with asymmetric swallow-tail alkyl group on one of its bpy ligands provides a good alternative for red-orange light generation. Nonetheless, according to our knowledge, luminous efficiency of 7 cd/A at a current density of 10 mA/cm^2, is one of the best results obtained by the use of Ru(II) complexes [24,29,30].

2. Experimental

2.1. Materials

Ruthenium(III) chloride hydrate and 1-bromohexane, were purchased from Fluka. *n*-Butyllithium (1.6 M in hexane),

* Corresponding author. Tel.: +90 232 311124; fax: +90 232 3886027.
E-mail addresses: onerilker@gmail.com (I. Oner), cigdemsahin82@gmail.com (C. Sahin), canan.varlikli@ege.edu.tr (C. Varlikli).

0143-7208/$ – see front matter © 2012 Elsevier Ltd. All rights reserved.
doi:10.1016/j.dyepig.2012.02.017

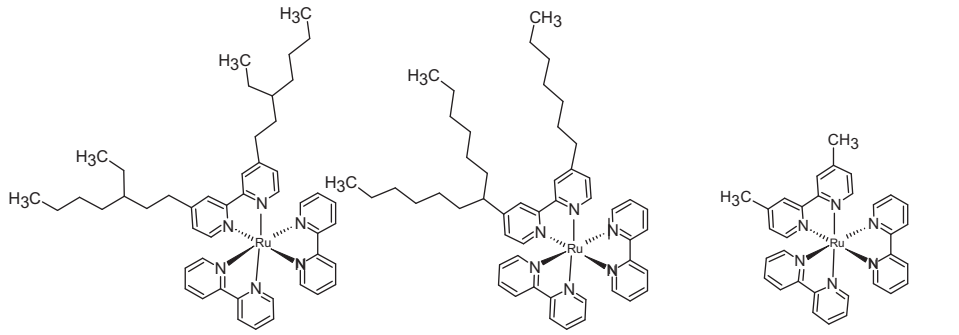

Fig. 1. Molecular structures of the complexes CS91, CS93 and $Ru(bpy)_2(dmbpy)$ $(PF_6)_2$.

4,4′-dimethyl-2,2′-bipyridine (dmbpy) and 2,2′-bipyridine were provided from Aldrich. Diisopropylamine and analytical grade solvents were obtained from Merck. $[Ru(bpy)_2Cl_2]\cdot 2H_2O$ and $[Ru(bpy)_2(dmbpy)](PF_6)_2$ were prepared according to the literature methods [31,32]. All reactions were carried out using standard Schlenk techniques under argon atmosphere. Poly(3,4-ethylenedioxythiophene):poly(styrene sulfonate) (PEDOT:PSS), poly (N-vinylcarbazole) (PVK) (M_w 1.100.000), 2-(4-Biphenylyl)-5-phenyl-1,3,4-oxadiazole (PBD), 4-(dicyanomethylene)-2-methyl-6-(4-dimethylaminostyryl)-4H-pyran (DCM), tetrabutylammoniumhexafluorophosphate ($TBAPF_6$) and 2,2,2-(1,3,5-benzenetriyl) tris-(1-phenyl-1H-benzimidazole) (TPBi) were purchased from Aldrich and Lum Tec Co., respectively and were used as received. ITO glass substrates were purchased from Delta Technologies.

2.2. Instruments

NMR spectra were recorded at probe temperature on Varian Mercury AS 400 NMR instrument at 400 MHz (1H), 100.56 MHz (13C) 162 MHz (31P), 376 (19F). Elemental analyses were performed by using a Carlo Erba 1106 elemental analyzer. Mass spectra were recorded on a Bruker Esquire 6000 ESI spectrometer and methanol was used as the mobile phase. Electrochemical data were obtained by using a CH Instrument 660 B Model electrochemical workstation. The thermal properties of the complexes were measured by thermal gravimetric analyzer (Perkin Elmer Pyris 6 TGA) and differential scanning calorimeter (Perkin Elmer Pyris 6 DSC) under nitrogen atmosphere. The absorption and photoluminescence (PL) properties were investigated with Analytik Jena S 600 UV and PTI-QM1 luminescence spectrophotometers, respectively. Fluorescence microscope images of thin films on glass were taken with Olympus IX71 inverted fluorescence microscope. The current–voltage (I–*V*) characteristics were measured with a Keithley 2400 programmable power source controlled by a LabView™ program. The EL spectra were obtained through the transparent glass substrate by the use of an Ocean Optics USB4000 fiber optic spectrometer with an optical fiber that was attached above the OLED normal to the glass substrate. Devices were tested in a glove box at room temperature without encapsulation.

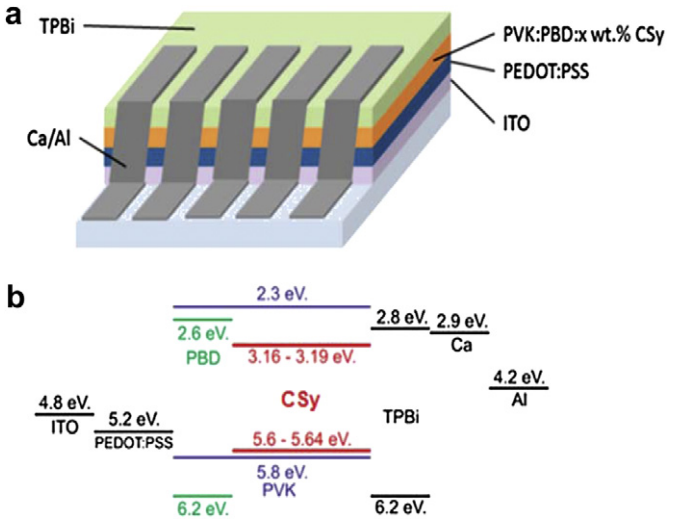

Fig. 2. Device illustration (a) and corresponding HOMO–LUMO energy diagram (b).

2.3. Synthesis of ligands and corresponding complexes

2.3.1. Synthesis of 4,4′-bis(3-ethylheptyl)-2,2′-bipyridine (L_1)

4,4′-(3-ethylheptyl)-2,2′-bipyridine was prepared according to the literature [33]. The product was chromatographed on neutral Al_2O_3 by the use of hexane/ether (10:1, v/v) as an eluent. Light yellow oily L_1 was obtained as the first fraction collected from column. Yield: 11%. ^{1}H NMR ($CDCl_3$) δ ppm: 8.56 (d, $J = 5.2$ Hz, 2H), 8.24 (s, 2H), 7.14 (dd, $J = 1.2$ Hz, 2H), 2.67 (m, 4H), 1.64 (m, 4H), 1.34 (m, 18 H), 0.89 (m, 12 H). ^{13}C NMR ($CDCl_3$) δ ppm: 156.5, 153.6, 149.2, 124.1, 121.5, 39.0, 34.4, 33.0, 29.1, 25.9, 23.3, 14.3, 11.0.

2.3.2. Synthesis of 4-dihexylmethyl-4′-heptyl-2,2′-bipyridine (L_2)

4-Dihexylmethyl-4′-heptyl-2,2′-bipyridine was synthesized according to the literature [34]. The product was purified on neutral Al_2O_3 by the use of hexane/ether (20:1, v/v) as an eluent. The light yellow oily L_2 was obtained as the second fraction collected from column. Yield: 25%. ^{1}H NMR ($CDCl_3$) δ ppm: 8.56 (d, $J = 5.2$ Hz, 2H), 8.25 (s, 1H), 8.19 (s, 1H), 7.12 (dd, $J = 1.6$ Hz, 1H), 7.09 (dd, $J = 1.6$ Hz, 1H), 2.69 (t, 2H), 2.59 (m, 1H), 1.64 (m, 6H), 1.22 (m, 24H), 0.85 (m, 9H). ^{13}C NMR ($CDCl_3$) δ ppm: 158.8, 156.9, 156.5, 156.4, 153.1, 149.2, 124.1, 123.4, 121.6, 120.9, 46.3, 36.5, 35.8, 32.0, 31.9, 30.7, 29.6, 29.5, 29.3, 27.8, 22.8, 22.8, 14.3, 14.2.

2.3.3. Synthesis of $[Ru(bpy)_2(L_1)](PF_6)_2$ (CS91)

$[Ru(bpy)_2Cl_2]\cdot 2H_2O$ (50 mg, 0.1 mmol) and L_1 (42 mg, 0.1 mmol) were heated under reflux in ethanol (15 ml) for 4 h under argon atmosphere. After cooling to room temperature, saturated aqueous solution of NH_4PF_6 was added into the reaction mixture and the precipitate was collected by filtration. The crude product was washed with water and diethyl ether. The orange solid was obtained with a yield of 96%. Melting point: 136 °C. FTIR (KBr, cm^{-1}): 2956, 2926, 2859 (C–H), 1614, 1538, 1420, 1375 (bpy). ^{1}H NMR (DMSO-d_6) δ ppm: 8.82 (d, $J = 8.2$ Hz, 4H), 8.75 (s, 2H), 8.15 (t, $J = 7.6$ Hz, 4H), 7.70 (d, $J = 5.2$ Hz, 4H), 7.52 (m, 6H), 7.38

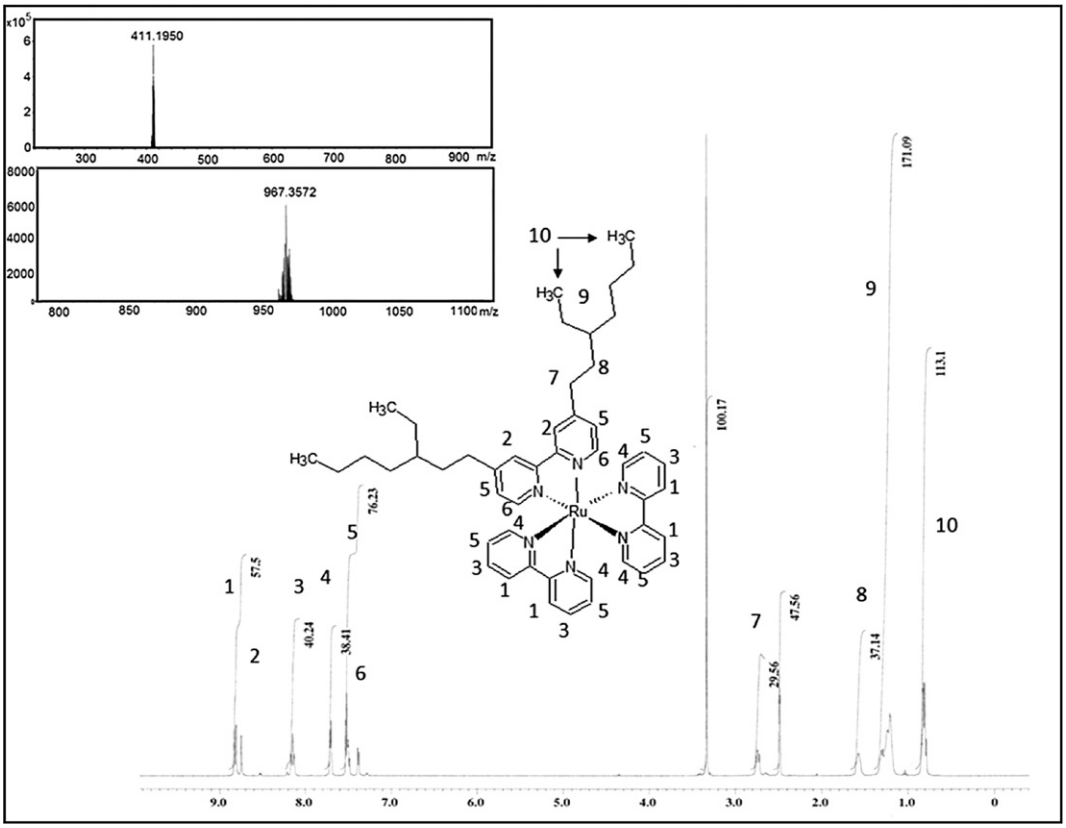

Fig. 3. ^{1}H NMR (solv. CD_3OD) and ESI mass spectra (inset) of CS91 dissolved in methanol.

(d, $J = 4.9$ Hz, 2H), 2.74 (t, $J = 8.1$ Hz, 4H), 1.58 (m, 4H), 1.24 (m, 18H), 0.82 (m, 12H). ^{19}F NMR (Acetone-d_6) δ ppm: −68.6 (d, $^{1}J_{P-F} = 708$ Hz). ^{31}P NMR (Acetone-d_6) δ ppm: 78.9 (sept., $^{1}J_{P-F} = 708$ Hz). ESI-MS (m/z) $[M-PF_6^-]^+$967.36, $[M-2PF_6^-]^{2+}$ 411.20. Elemental distribution calculated for $C_{48}H_{60}N_6P_2F_{12}Ru$: C, 51.84%; H, 5.44%; N, 7.56%, and found: C, 51.81%; H, 5.38%; N, 7.60%.

2.3.4. Synthesis of $[Ru(bpy)_2(L_2)](PF_6)_2$ (CS93)

CS93 was synthesized using the same reaction conditions and purification steps of CS91 except that; L_2 was used instead of L_1. Yield 97%. FTIR (KBr, cm^{-1}): 2926, 2855 (C–H), 1614, 1540, 1422, 1376 (bpy). ^{1}H NMR (DMSO-d_6) δ ppm: 8.82 (m, 5H), 8.71 (s, 1H), 8.15 (m, 4H), 7.70 (d, 4H), 7.52 (m, 6H), 7.35 (t, 2H), 2.75 (m, 3H), 1.64 (m, 6H), 1.22 (m, 24H), 0.80 (m, 9H). ^{19}F NMR (Acetone-d_6) δ ppm: −68.6 (d, $^{1}J_{P-F} = 708$ Hz). ^{31}P NMR (Acetone-d_6) δ ppm: 78.9 (sept., $^{1}J_{P-F} = 708$ Hz). ESI-MS (m/z) $[M-PF_6^-]^+$995.39, $[M-2PF_6^-]^{2+}$ 425.21. Elemental distribution calculated for $C_{50}H_{64}N_6P_2F_{12}Ru$: C, 52.68%; H, 5.66%; N, 7.37%, and found: C, 52.78%; H, 5.65%; N, 7.42%.

Structures of the synthesized complexes are given in Fig. 1 together with the structure of $Ru(bpy)_2(dmbpy)(PF_6)_2$.

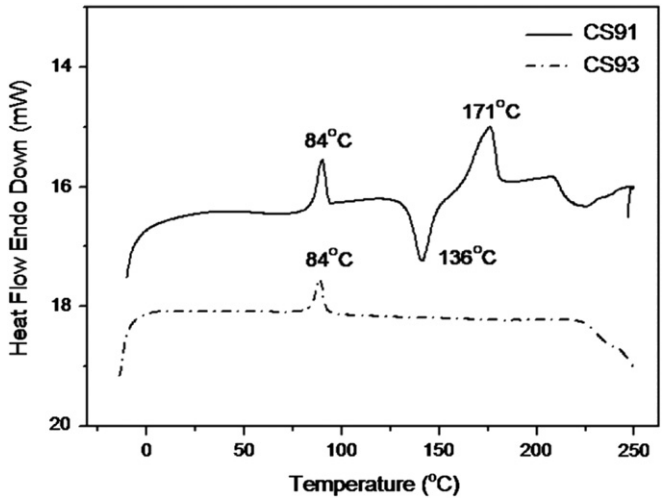

Fig. 4. DSC thermograms of CS91 and CS93.

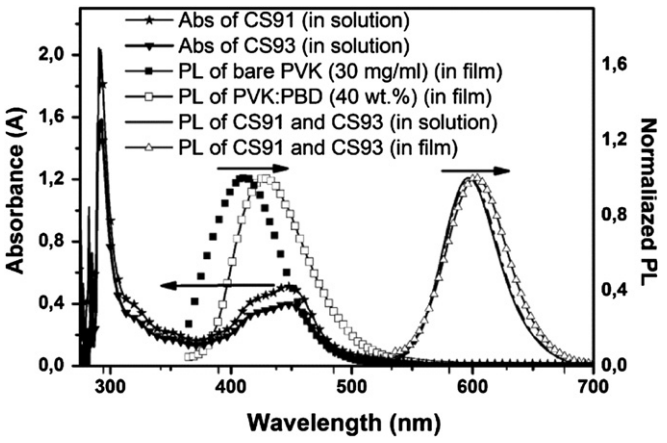

Fig. 5. UV–Vis absorption spectra of CS91 and CS93 at the same concentration in 1,2-dichlorobenzene and normalized PL spectra of them together with the bare PVK and PVK:PBD (40 wt.%) in thin film.

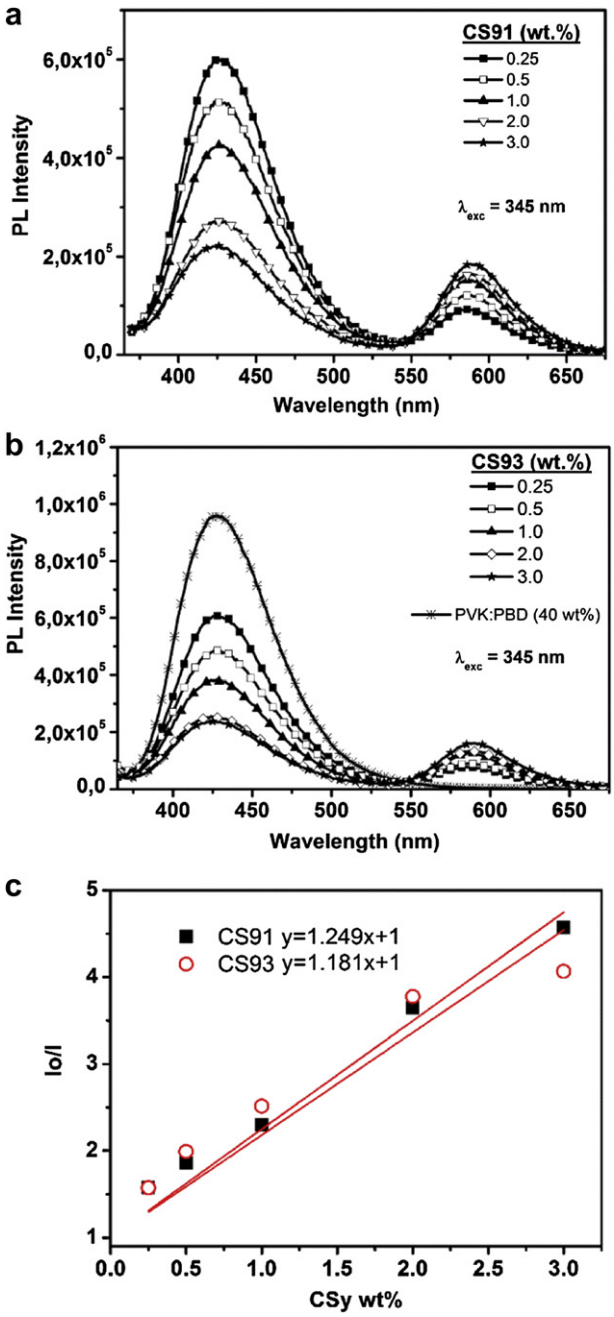

Fig. 6. Photoluminescence spectra of (a) PVK:PBD:*x* wt.% CS91 and (b) PVK:PBD (40 wt.%) PVK:PBD:*x* wt.% CS93 thin films (*x*: 0.25, 0.5, 1, 2, 3) and (c) corresponding Stern–Volmer plots.

2.4. Preparation and characterization of OLEDs

ITO coated glass substrates ($\rho = 4$–$10\ \Omega/\square$) were etched and ultrasonically cleaned in acetone and isopropanol for 15 min each, and blow dried with high purity nitrogen. Prior to coating the organic materials, they were treated by O_2 plasma for 2 min. Conductive polymer layer (PEDOT:PSS) was coated onto ITO substrates at 4000 rpm which yields a 40 nm film thickness. Light emitting layer (80 nm) was spin-coated from 1,2-dichlorobenzene solution that contains 30 mg/ml of *x* wt.%CS*y* (*x*: 0.25, 0.5, 1, 2, 3 wt.%; *y*: 91 or 93) in PVK:PBD (40 wt.%) host on PEDOT:PSS coated ITO glass. TPBi (40 nm) was deposited by thermal evaporation (Nanomaster NTE3000) at a rate of 0.4 Å/s. Finally, Ca (40 nm) and Al (100 nm) cathodes were deposited through a shadow mask by the use of a vacuum evaporator, attached to a MBRAUN 200B glove box system, at a rate of 0.5 Å/s and 0.8 Å/s, respectively. Before the deposition of TPBi, the films were heat treated at 80 °C for 1 h in a vacuum oven. A control device that would contain $[Ru(bpy)_2(dmbpy)](PF_6)_2$ was also planned but low solubility (solubility = 0.7 mg/ml in 1,2-dichlorobenzene) of this material forestalled its film studies and OLED application. The active area was $4 \times 3\ mm^2$ and five parallel measurements were performed for each device. The device illustration and the corresponding HOMO–LUMO energy diagram are shown in Fig. 2.

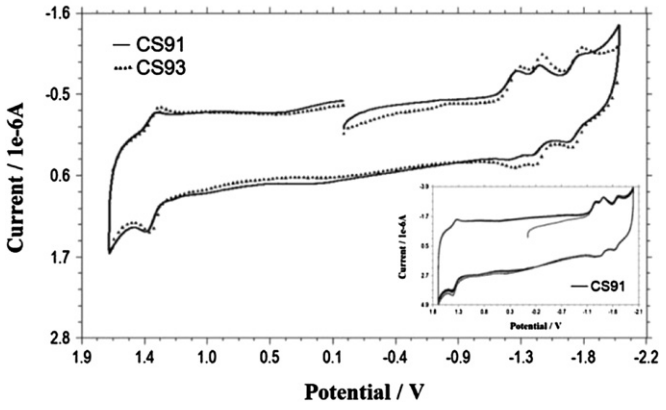

Fig. 7. Cyclic voltammograms of the CS91 and CS93 measured in acetonitrile and inset is the five consecutive cyclic voltammograms of complex CS91 in acetonitrile solution; scan rate is 100 mV s^{-1}.

3. Results and discussion

3.1. Structural, spectral and electrochemical analysis

3.1.1. Structural characterization

The ratios of aromatic resonance peaks in the ^1H NMR spectra of CS91 (Fig. 3) and CS93 proved the presence of three bipyridine ligands. The resonance peak at 0.81 ppm is assigned to 12 protons of 4 methyl groups in CS91, while aliphatic resonance peak of 3 methyl groups in CS93 appeared at 0.82 ppm. The presence of PF_6^- anion is confirmed with ^{31}P and ^{19}F NMR spectroscopies. ^{31}P NMR spectrum gave septet peak observed at 78.9 ppm corresponding to the P atom due to the interaction of P and F atoms and ^{19}F NMR also shows doublet peak at −68.6 ppm for CS91 and CS93. The ESI mass spectrum of complex CS91 is shown in Fig. 3. The measured values of CS91 for $[M-PF_6^-]^+$ and $[M-2PF_6^-]^{2+}$ are at 967.3572 and,

Table 1
The electrochemical data of the complexes in acetonitrile.

Complex	E_{ox}^{onset} (V)	E_{red1}^{onset} (V)	E_{red2} (V)	E_{red3} (V)	HOMO (eV)	LUMO (eV)	Band gap (ΔE_g)(V)
$[Ru(bpy)_2(dmbpy)](PF_6)_2$	1.36	−1.09	−1.38	−1.65	−5.67	−3.22	2.45
CS91	1.33	−1.12	−1.42	−1.70	−5.64	−3.19	2.45
CS93	1.29	−1.16	−1.45	−1.73	−5.60	−3.15	2.45

411.1950 m/z which are in agreement with the calculated values of 967.3582 and 411.1962 m/z, respectively.

TGA thermograms of CS91 and CS93 present weight losses starting at 248 °C and 257 °C, respectively. DSC thermograms of both of the complexes give crystallization peak at 84 °C but a melting point of 136 °C is observed only for CS91. Furthermore, CS91 gives a broad peak between 156 °C and 176 °C (maximum point of peak at 171 °C) which is attributed to temperature dependent aggregation of CS91 (Fig. 4) [34]. Regarding the stereochemistry there is a structural difference between CS91 and CS93 as the former has a chirality that is located in lateral alkyl chains of 4,4′-bis(3-ethylheptyl)-2,2′-bipyridine. Such chiral alkyl chains may be the reason of higher tendency to form aggregates [35,36].

3.1.2. Absorption and emission studies

UV–Vis absorption and normalized PL spectra of CS91 and CS93 in 1,2-dichlorobenzene solutions and films are shown in Fig. 5 together with bare PVK and PVK:PBD (40 wt.%) blend films. The absorption spectra of the two complexes are almost the same. The strong absorption peaks centered at 297 nm generated from the $\pi-\pi^*$ ligand centered charge transfer (LC) transitions of bpy ligands and broad absorption bands between 380 and 550 nm are assigned to metal to ligand charge transfer (MLCT) [37]. Both of the complexes give orange-red ^{3}MLCT emission centered at 598 nm in solution. Independent from the dopant nature a negligible bathochromic shift is observed in their films due to the $\pi-\pi$ stacking of the molecules in solid state. The relative fluorescence quantum yields (Φ_f) of CS91 and CS93 in 1,2-dichlorobenzene are calculated by the use of equation given in literature [38] and 4-(dicyanomethylene)-2-methyl-6-(4-dimethylaminostyryl)-4H-pyran (DCM) as reference ($\Phi_f^{Methanol} = 0.38$ at $\lambda_{ext} = 460$ nm) [39]. The PL of Ru(II)bpy type materials are known to be oxygen sensitive [40,41], therefore N_2 saturated solutions were used in the measurements. The calculated Φ_f values were 0.14, 0.16 and 0.14 for CS91, CS93 and $[Ru(bpy)_2(dmbpy)](PF_6)_2$, respectively. Structural difference in alkyl chains of CS91 and CS93 did not make a significant effect on photoluminescence properties. However, the molar absorptivity constants (ε) that corresponds to the MLCTs of CS91 and CS93 were slightly different; 1.56×10^4 M^{-1} cm^{-1} and 1.19×10^4 M^{-1} cm^{-1}, respectively.

The blend of PVK and PBD which have balanced charge transporting ability is selected as the host [29]. The reason for choosing PVK:PBD blends, rather than PVK itself, is the better overlap of the PL of the blend with the absorption spectra of complexes (Fig. 5). A better match in the donor PL and acceptor absorption would result in a better energy transfer. The red shift observed in the blend

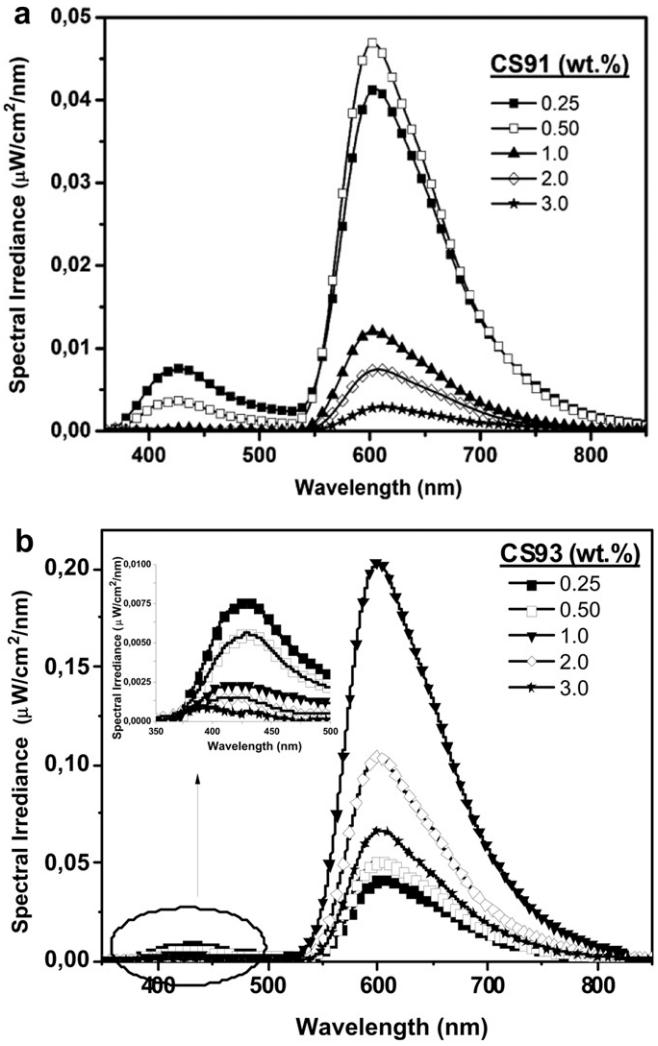

Fig. 8. Influence of doping ratio on electroluminescence of CS91 (a) and CS93 (b) based devices ($V_{apl.} = 15$ V).

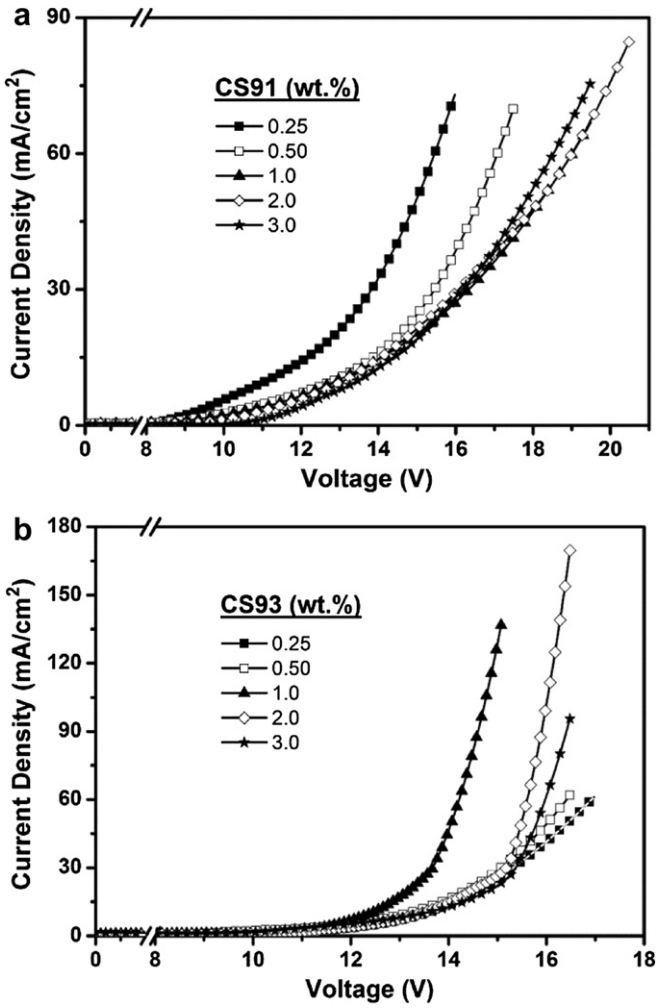

Fig. 9. Influence of doping ratio on current density–voltage characteristics of CS91 (a) and CS93 (b) doped devices.

Table 2
Performance characteristics for ITO/PEDOT:PSS/PVK:PBD(40 wt.%):*x*%CS*y*/TPBi/Ca/Al devices.

X conc. [wt.%]	Luminance[a] [cd m^{-2}]		Luminous efficiency [cd A^{-1}]		Power efficiency [lm W^{-1}]		Quantum efficiency [%]		Turn-on voltage [V]		λ_{max} [nm] CIE (*x*,*y*)	
	CS91	CS93	CS91	CS93	CS91	CS93	CS91	CS93	CS91	CS93	CS91	CS93
0.25	1157	395	1.4	1.8	0.3	0.4	0.1	0.12	9.0	9.5	427, 603 *(0.53,0.35)*	427, 600 *(0.44,0.31)*
0.50	1507	1215	2.8	3.6	0.5	0.8	0.17	0.21	9.2	9.0	427, 603 *(0.56,0.37)*	427, 600 *(0.55,0.37)*
1	1529	3824	2.7	7.0	0.4	1.7	0.13	0.39	11.0	8.5	427, 603 *(0.59,0.38)*	427, 600 *(0.57,0.39)*
2	789	3536	1.2	5.8	0.2	1.3	0.07	0.34	11.2	8.7	607 *(0.60,0.38)*	600 *(0.59,0.39)*
3	344	3426	0.3	3.2	0.07	0.7	0.03	0.2	11.5	9.8	612 *(0.61,0.37)*	600 *(0.59,0.39)*

[a] Values at the driving voltage of 15 V.

compared to bare PVK is due to the exciplex tendency of oxadiazole and carbazole groups [42].

Photo-induced donor–acceptor relationship between PVK:PBD blend and CS*y* is observed by increasing wt.%CS*y* in the blend film (Fig. 6). A drastic decrease in overall intensity of the PVK:PBD emission and a simultaneous peak evolution at 590 nm is observed which implies an energy transfer from PVK:PBD to CS*y*. With increasing the concentration of complexes (from 0.25 to 3 wt.%), further decrease in the emission peak of PVK:PBD host is observed. However PVK:PBD emission in PVK:PBD:Ru film could not be completely quenched which indicates that a complete energy transfer did not take place. Still, the slightly higher ε value of CS91 denotes the probability of a better energy transfer as the overlap integral of PVK:PBD blend photoluminescence and CS91 absorption is higher than that of CS93. This is supported by the application of PL quenching data in the Stern–Volmer equation [43]:

$$I_M/I_{QM} = 1 + K_{QM}[Q]$$

where I_M/I_{QM} is the ratio of measured PL intensity of PVK:PBD blend in the absence and presence of CS*y*, K_{QM} is the Stern–Volmer coefficient and [*Q*] is the concentration of CS*y* in the film. Therefore, the slope of I_M/I_{QM} *vs.* [*Q*] curve is equal to K_{QM}. The obtained K_{QM} values were 1.249 and 1.181 for the quenching experiments performed with CS91 and CS93, respectively (Fig. 6c).

3.1.3. Electrochemical properties

Electrochemical properties of the materials used in photochemical molecular devices, including OLEDs, are very important for the design of the device structure. The electrochemical studies

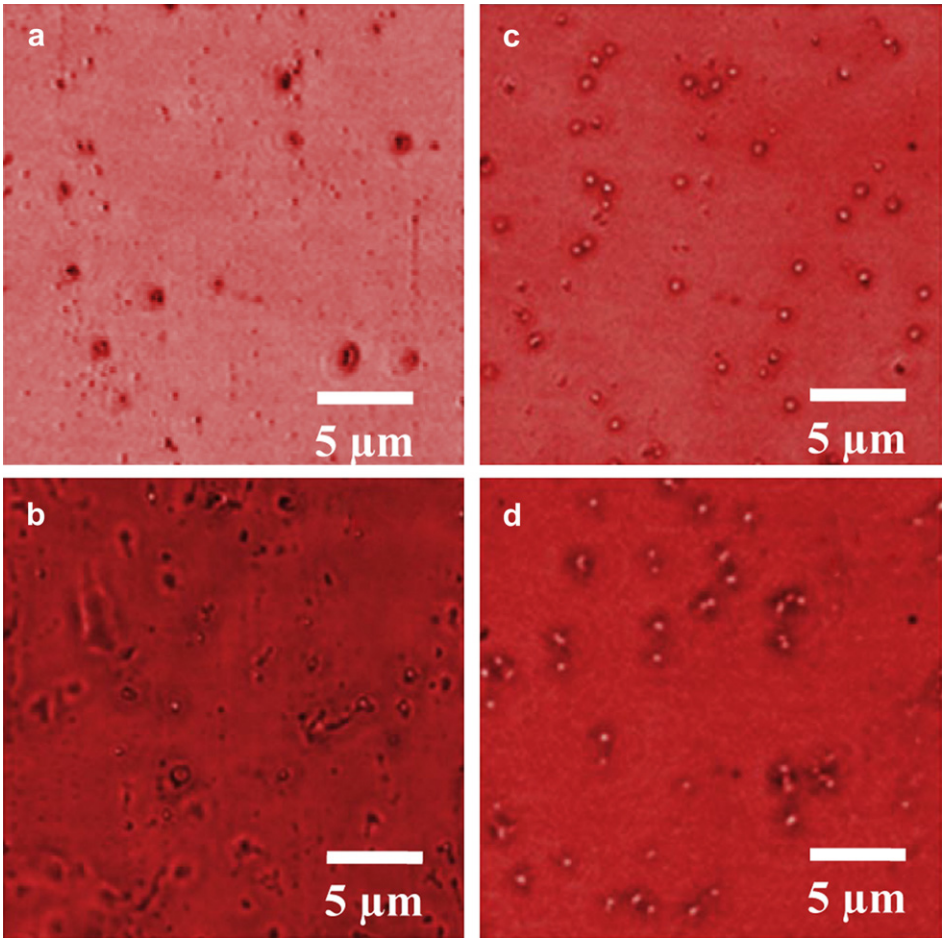

Fig. 10. Fluorescence microscope images of spin-coated (a) 1 wt.%, (b) 3 wt.% CS91 doped and (c) 1 wt.%, (d) 3 wt.% CS93 doped PVK:PBD blend thin films.

of CS91 and CS93 were performed by using glassy carbon working electrode, Pt wire counter electrode and Ag wire reference electrode in acetonitrile solvent that contains 0.1 M $TBAPF_6$. The redox potentials are summarized in Table 1. The cyclic voltammograms of CS91 and CS93 (Fig. 7) showed one reversible oxidation peak and three reduction peaks. The reversible oxidation peak of CS91 and CS93 are observed at 1.33 V and 1.29 V *vs.* Ag/Ag^+, respectively and are assigned to Ru(II)/Ru(III) couple. Three reversible reduction peaks of the complexes are attributed to each of the two bpy ligands and bpy ligand with alkyl groups (L_1 and L_2), respectively. The oxidation and reduction potentials of CS93 are slightly shifted to the cathodic area due to the presence of more donor L_2 which contains the branched swallow-tail alkyl substituent at the first exocyclic carbon of 4,4′-dimethyl-2,2′-bipyridine when compared to CS91. The onset of the first oxidation and reduction potentials and ferrocene as an internal standard are used to determine the HOMO and LUMO energy level of complexes [44]. The onset of the ferrocene peak is at 0.49 V *vs.* Ag/Ag^+. The calculated HOMO and LUMO energy levels for CS91 and CS93 are 5.64 eV, 5.60 eV and 3.19 eV, 3.16 eV, respectively. If the overall evaluation of the data given in Table 1 is made, one may conclude that with the increase in electron donor ability of the alkyls on bpy ligand, both HOMO and LUMO energy levels come closer to the vacuum level; however the electrochemical band gap does not change. In order to control electrochemical stability of CS*y* several consecutive voltammograms were performed and no significant change in peak currents and potentials of anodic and cathodic areas are observed (Fig. 7 – inset).

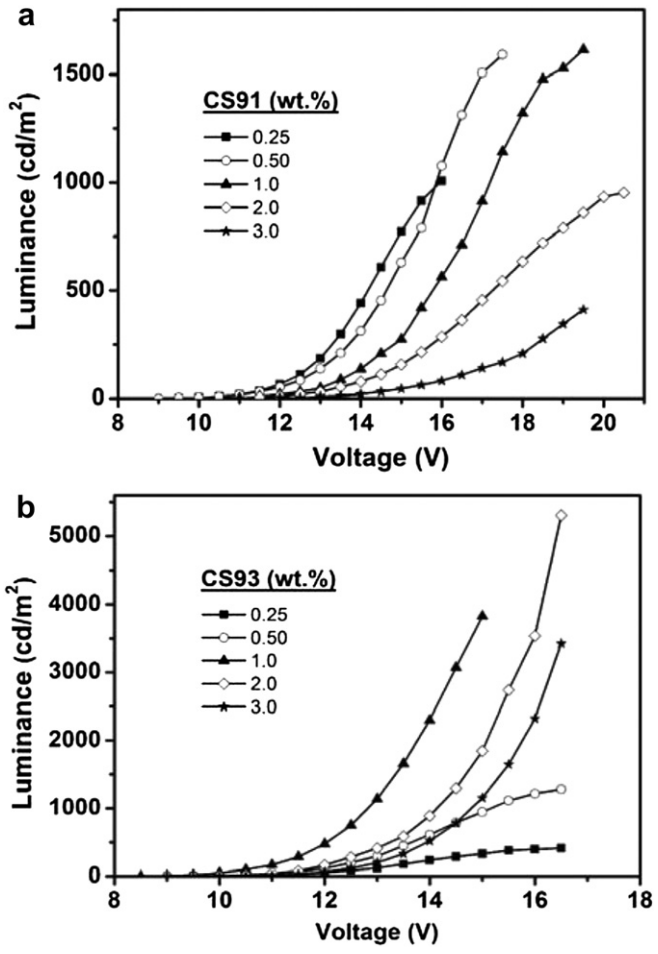

Fig. 11. Luminance–voltage curves of CS91 (a) and CS93 (b) based devices.

3.2. OLED performance

The electroluminescence spectra and current density–voltage (*J–V*) curves of the devices that contain CS91 and CS93 are shown in Figs. 8 and 9, respectively. Fig. 8 shows the actual values of spectral irradiance obtained from the devices at applied voltage of 15 V. The maximum EL intensity at around 600 nm is 4 times higher in CS93 doped device than that of CS91. The weak emission in the region of 350–500 nm originated from the PVK:PBD exciplex. The 350–500 nm region of Fig. 8b is enlarged as an inset in order to make it easier to notice that the EL intensities of PVK:PBD in both of the devices were almost the same. Therefore, regarding the energy transfer efficiency, unlike the situation in PL, donor–acceptor relationship between PVK:PBD and CS*y* are the same. A complete quenching of emission obtained from the host system was reached at 1 wt.%CS*y* doping. The mechanism of EL obtained from similar systems that presents different PL and EL properties is proposed as charge trapping and supported by turn-on voltage ($V_{turn\text{-}on}$) increase and current density (*J*) decrease with the increase in dopant concentration [26]. This behavior is valid in the case of CS91 from 0.25 wt.% up to 3 wt.% and CS93 following 1 wt.% doping. For doping concentrations of higher than 1 wt.% in CS91 based devices no significant change in *J* and $V_{turn\text{-}on}$ values is detected. However, EL maximum of these devices made a bathochromic shift of 9 nm

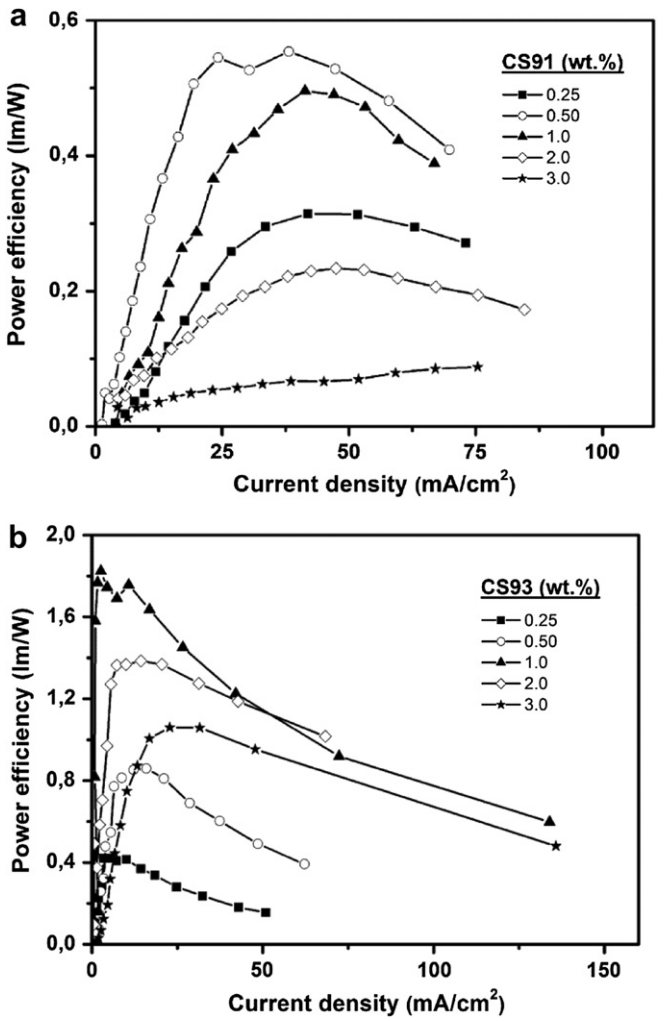

Fig. 12. Power efficiency–current density curves of CS91 (a) and CS93 (b) based devices.

while that of CS93 remained constant (Table 2). This indicates that the branching of the alkyl substituent at the first exocyclic carbon of bpy ligand, lowers the tendency of the Ru(II) complex to aggregate and increase its compatibility with the host. In addition to the discussions made on DSC thermograms, this conclusion is also supported by higher *J* obtained in CS93 based devices [45].

Recently, the use of optical microscopy techniques has made it possible to study physical properties of materials [46,47]. Fig. 10 shows the fluorescence microscope images of 1 and 3 wt.% CS91 and CS93 doped PVK:PBD films prepared at the same conditions used in device preparation, and excited with blue light (λ_{ext} = 470–490 nm). Aggregates are clearly seen in all images, whereas the image spots are much bigger in CS91 doped PVK:PDB films than that of CS93. The image spots increase with increasing dopant concentration. This feature indicates that relatively poor efficiencies of CS91 doped devices (Table 2) may have been induced by phase separation, and highly aggregated CS91 molecules act as trapping centers for the injected charges [47].

The performance characteristics of ITO/PEDOT:PSS/PVK:PBD(40 wt.%):*x* wt.%CSy/TPBi/Ca/Al devices are listed in Table 2. The highest luminous and power efficiency and lowest turn-on voltage values are obtained from the 1 wt.% CS93 doped device as 7.0 cd/A and 1.7 lm/W at 10 mA/cm^2 and 8.5 V, while that of 0.5 wt.% CS91 doped device are 2.8 cd/A and 0.5 lm/W at 10 mA/cm^2 and 9.2 V, respectively. The efficiencies gained from the 1 wt.% CS93 doped device are one of the best results obtained from the devices with similar structures [26,28,30]. The maximum brightness obtained from this device is 3824 cd/m^2 which is 2 folds higher than the best value that could be reached with CS91 doped examples. The high turn-on and driving voltages may be due to the relatively high thickness of the emissive layer (80 nm) and large hole barrier at the PEDOT:PSS/PVK:PBD interface [48]. However, the obtained turn-on and driving voltages are comparable and lower than with those of literature values [23–26,29]. All devices emit orange-red light and Commission Internationale de L'Eclairage color coordinates (CIE) remained constant with applied voltage.

The luminance − *V*, power and luminous efficiency − *J* characteristics of the devices are shown in Figs. 11–13, respectively. Compared with CS91 doped devices, higher luminance, power and luminous efficiency are observed at the same applied voltage withCS93 doped devices. The power and luminous efficiency of CS93 decreases faster with the increase in *J* which may be attributed to the faster increase of triplet–triplet (T–T) annihilation and field-induced quenching effects [26]. However, even at high current densities, the power efficiency values of the 1 wt.% CS93 doped device is higher than that of the best device performance that could

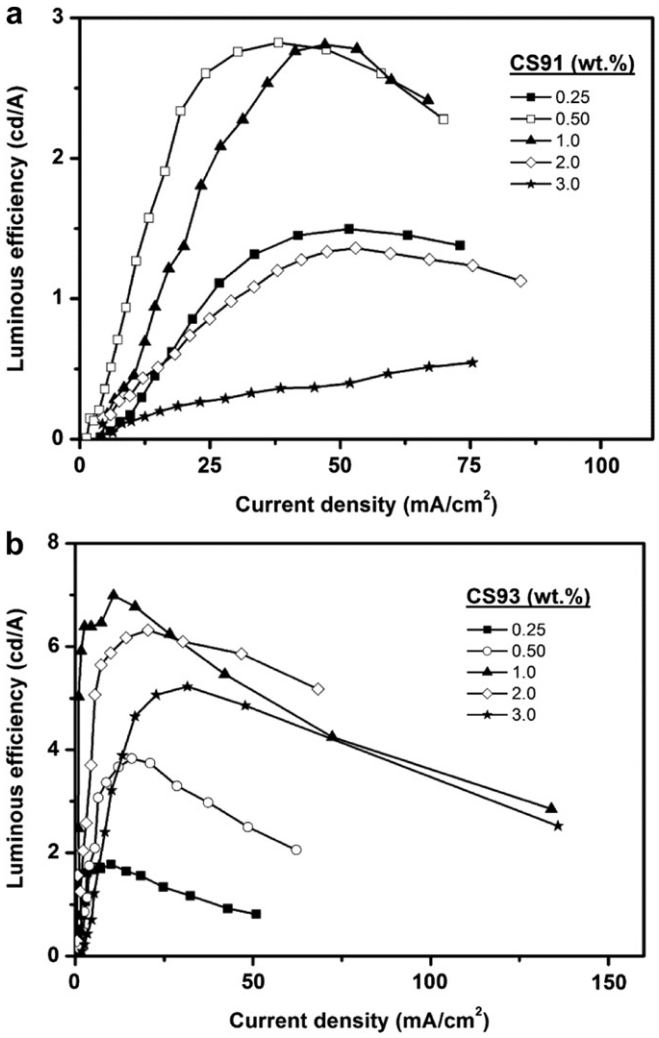

Fig. 13. Luminous efficiency–current density curves of CS91 (a) and CS93 (b) doped devices.

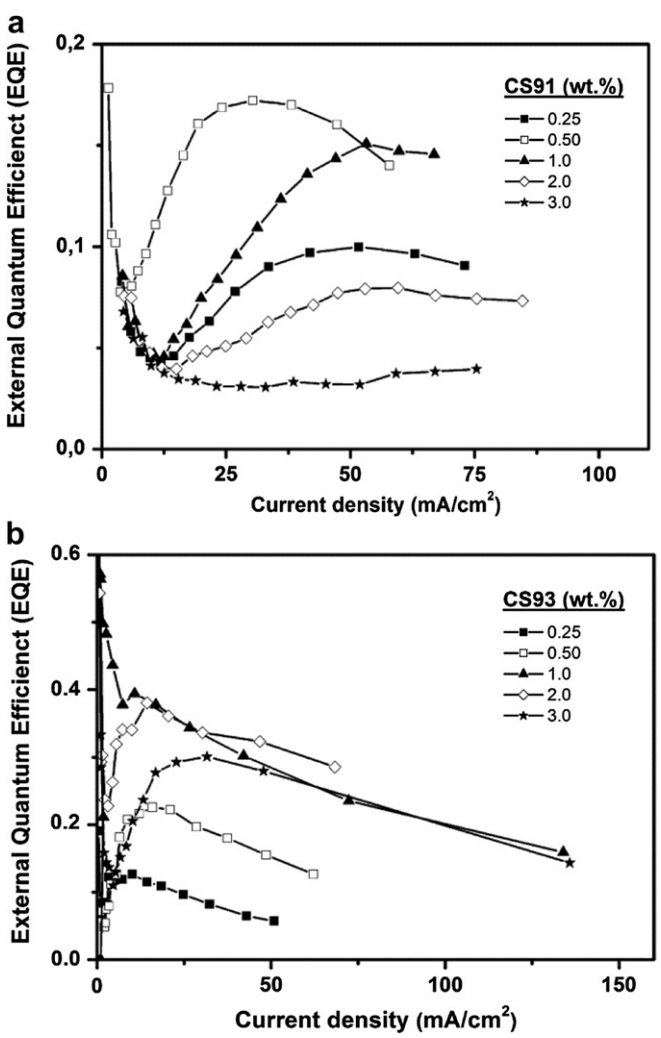

Fig. 14. External quantum efficiency–current density curves of CS91 (a) and CS93 (b) doped devices.

be reached by CS91 doping. This shows that, CS93 is a better electroluminescent phosphor for OLED devices.

Fig. 14 shows the external quantum efficiency (EQE) *vs*. *J* characteristics of the devices. The device with 0.5 wt.% CS91 and the device with 1 wt.% CS93 achieved an EQE of 0.17% and 0.39% at 10 mA/cm^2. The slow decrease in EQE of both devices can be attributed to the alkyl chain on the bipyridyl ligand which suppress the T–T annihilation due to better chemical compatibility and more homogenous distribution of the ruthenium molecules in the PVK:PBD matrix [26]. The higher EQE observed for CS93 doped devices are due to decreased aggregation and self-quenching of the CS93 with branched alkyl substituents from the first exocyclic carbon of bpy ligand.

4. Conclusion

In this paper, the synthesis, photophysical, thermal and electrochemical properties of two new Ru(II) complexes and their electroluminescence (EL) characteristics when employed as a dopant in ITO/PEDOT:PSS/PVK:PBD(40 wt.%):*x*%CS*y*/TPBi/Ca/Al device are reported. Although the difference of the alkyl substituent on the bpy ligand did not have a significant effect on ground state absorption and PL properties, EL efficiencies were more than 2 folds higher for the complex that contained the swallow-tail alkyl substituent at the first exocyclic carbon. However, the significance of this study should be supported by further transient studies.

Acknowledgments

We acknowledge the project support funds of EAE Lighting Company, Ege University and State Planning Organization of Turkey (DPT). We thank Prof. Dr. Serdar Ozcelik and Gulcin Unal from Izmir Institute of Technology, Turkey for the fluorescence microscopy images.

References

[1] Xiao L, Chen Z, Qu B, Luo J, Kong S, Gong Q, et al. Recent progresses on materials for electrophosphorescent organic light-emitting devices. Advanced Materials 2011;23(8):926–52.
[2] Yersin H, Rausch AF, Czerwieniec R, Hofbeck T, Fischer T. The triplet state of organo-transition metal compounds. Triplet harvesting and singlet harvesting for efficient OLEDs. Coordination Chemistry Reviews 2011;255(21–22):2622–52.
[3] Holder E, Langeveld BMW, Schubert US. New trends in the use of transition metal–ligand complexes for applications in electroluminescent devices. Advanced Materials 2005;17(9):1109–21.
[4] Wagenknecht PS, Ford PC. Metal centered ligand field excited states: their roles in the design and performance of transition metal based photochemical molecular devices. Coordination Chemistry Reviews 2011;255(5–6):591–616.
[5] Pentlehner D, Grau I, Yersin H. Triplet state properties of [Os(phen)2(dppene)] 2+ in different host materials and host to guest energy transfer in PVK. Chemical Physics Letters 2008;455(1–3):72–8.
[6] Tung Y-L, Lee S-W, Chi Y, Tao Y-T, Chien C-H, Cheng Y-M, et al. Organic light-emitting diodes based on charge-neutral Os(ii) emitters: generation of saturated red emission with very high external quantum efficiency. Journal of Materials Chemistry 2005;15(4):460–4.
[7] Ulbricht C, Beyer B, Friebe C, Winter A, Schubert US. Recent developments in the application of phosphorescent iridium(III) complex systems. Advanced Materials 2009;21(44):4418–41.
[8] Wu W, Cheng C, Wu W, Guo H, Ji S, Song P, et al. Tuning the emission colour of triphenylamine-capped cyclometallated platinum(II) complexes and their application in luminescent oxygen sensing and organic light-emitting diodes. European Journal of Inorganic Chemistry 2010;29:4683–96.
[9] Slinker JD, Rivnay J, Moskowitz JS, Parker JB, Bernhard S, Abruna HD, et al. Electroluminescent devices from ionic transition metal complexes. Journal of Materials Chemistry 2007;17(29):2976–88.
[10] Juris A, Balzani V, Barigelletti F, Campagna S, Belser P, von Zelewsky A. Ru(II) polypyridine complexes: photophysics, photochemistry, electrochemistry, and chemiluminescence. Coordination Chemistry Reviews 1988;84:85–277.
[11] Zhu Y, Gu C, Tang S, Fei T, Gu X, Wang H, et al. A new kind of peripheral carbazole substituted ruthenium(II) complexes for electrochemical deposition organic light-emitting diodes. Journal of Materials Chemistry 2009;19(23): 3941–9.
[12] Shiratori S. A quick operating organic EL device using Ru complex light-emitting layer with 2,5-bis(4-tert-butyl-2-benz-oxazolyl) thiophene electron transport layer. Materials Science and Engineering B 2001;85(2–3):149–53.
[13] Itoh N. Electrochemical light-emitting gel. Materials 2010;3(6):3729–39.
[14] Handy ES, Pal AJ, Rubner MF. Solid-state light-emitting devices based on the tris-chelated ruthenium(II) complex. 2. Tris(bipyridyl)ruthenium(II) as a high-brightness emitter. Journal of the American Chemical Society 1999;121(14): 3525–8.
[15] Maness KM, Terrill RH, Meyer TJ, Murray RW, Wightman RM. Solid-state diode-like chemiluminescence based on serial, immobilized concentration gradients in mixed-valent poly[Ru(vbpy)$_3$](PF$_6$)$_2$ films. Journal of the American Chemical Society 1996;118(43):10609–16.
[16] Elliott CM, Pichot F, Bloom CJ, Rider LS. Highly efficient solid-state electrochemically generated chemiluminescence from ester-substituted trisbipyridineruthenium(II)-based polymers. Journal of the American Chemical Society 1998;120(27):6781–4.
[17] Gao FG, Bard AJ. Solid-state organic light-emitting diodes based on tris(2,2′-bipyridine)ruthenium(II) complexes. Journal of the American Chemical Society 2000;122(30):7426–7.
[18] Rudmann H, Rubner MF. Single layer light-emitting devices with high efficiency and long lifetime based on tris(2,2[sup [prime]] bipyridyl) ruthenium(II) hexafluorophosphate. Journal of Applied Physics 2001;90(9):4338–45.
[19] Gao FG, Bard AJ. High-brightness and low-voltage light-emitting devices based on trischelated ruthenium(II) and tris(2,2′-bipyridine)osmium(II) emitter layers and low melting point alloy cathode contacts. Chemistry of Materials 2002;14(8):3465–70.
[20] Liu C-Y, Bard AJ. Individually addressable submicron scale light-emitting devices based on electroluminescence of solid Ru(bpy)$_3$(ClO$_4$)$_2$ films. Journal of the American Chemical Society 2002;124(16):4190–1.
[21] Wang T-J, Chen C-H, Chang S-M, Tzeng Y-J, Chao Y-C. Flexible polymer light-emitting devices based on ruthenium complexes. Microwave and Optical Technology Letters 2003;38(5):406–9.
[22] Yang J, Gordon KC. Light emitting devices from blended films of ruthenium(II) bis(2,2′-bipyridine)(4,7-dimethyl-1,10-phenanthroline) complex with poly(N-vinylcarbazole). Chemical Physics Letters 2003;372(3–4):577–82.
[23] Xia H, Zhang C, Qiu S, Lu P, Zhang J, Ma Y. Highly efficient red phosphorescent light-emitting diodes based on ruthenium(II)-complex-doped semiconductive polymers. Applied Physics Letters 2004;84(2):290–2.
[24] Xia H, Zhang C, Liu X, Qiu S, Lu P, Shen F, et al. Ruthenium(II) complex as phosphorescent dopant for highly efficient red polymers light-emitting diodes. The Journal of Physical Chemistry B 2004;108(10):3185–90.
[25] Yang J, Gordon KC. Electroluminescence of ruthenium(II)(4,7-diphenyl-1,10-phenanthroline)3 from charge trapping by doping in carrier-transporting blend films. Chemical Physics Letters 2004;385(5–6):481–5.
[26] Xia H, Zhu Y, Lu D, Li M, Zhang C, Yang B, et al. Ruthenium(II) complexes with the mixed ligands 2,2′-bipyridine and 4,4′-dialkyl ester-2,2′-bipyridine as pure red dopants for a single-layer electrophosphorescent device. The Journal of Physical Chemistry B 2006;110(37):18718–23.
[27] Santos G, Fonseca F, Andrade AM, Patrocínio AOT, Mizoguchi SK, Murakami Iha NY, et al. Development and characterization of light-emitting diodes (LEDs) based on ruthenium complex single layer for transparent displays. Physica Status Solidi (a) 2008;205(8):2057–60.
[28] Kim T-H, Yoo D-H, Park JH, Park OO, Yu J-W, Kim JK. Enhanced electrophosphorescence via highly efficient energy transfer from conjugated polymer. Applied Physics Letters 2005;86(17):171108–13.
[29] Yingying Z, Fangzhong S, Meirong L, Ming Z, Yuguang M. Highly efficient red phosphorescence from dopant polymer light emitting diodes based on mixed-ligand ruthenium(II) complex. Semiconductor Science and Technology 2008; 23(5):052001.
[30] Tung YL, Chen LS, Chi Y, Chou PT, Cheng YM, Li EY, et al. Orange and red organic light-emitting devices employing neutral Ru(II) emitters: rational design and prospects for color tuning. Advanced Functional Materials 2006; 16(12):1615–26.
[31] Sprintschnik G, Sprintschnik HW, Kirsch PP, Whitten DG. Photochemical reactions in organized monolayer assemblies. 6. Preparation and photochemical reactivity of surfactant ruthenium(II) complexes in monolayer assemblies and at water–solid interfaces. Journal of the American Chemical Society 1977;99(15):4947–54.
[32] Chuai Y, Lee DN, Zhen C, Min JH, Kim BH, Zou D. Novel polypyridyl ruthenium(II) complexes for electroluminescence. Synthetic Metals 2004; 145(2–3):259–64.
[33] Sahin C, Dittrich T, Varlikli C, Icli S, Lux-Steiner MC. Role of side groups in pyridine and bipyridine ruthenium dye complexes for modulated surface photovoltage in nanoporous TiO$_2$. Solar Energy Materials and Solar Cells 2010; 94(4):686–90.
[34] Sahin C, Tozlu C, Ocakoglu K, Zafer C, Varlikli C, Icli S. Synthesis of an amphiphilic ruthenium complex with swallow-tail bipyridyl ligand and its application in nc-DSC. Inorganica Chimica Acta 2008;361(3):671–6.
[35] Liu W, Guenet J-M, Green MM. Chiral effect on a self-assembling bicopper complex. Chirality 2004;16(9):661–4.
[36] Hofmeier H, El-ghayoury A, Schenning APHJ, Schubert US. Synthesis and optical properties of (a)chiral terpyridine-ruthenium complexes. Tetrahedron 2004;60(29):6121–8.
[37] Crosby GA, Watts RJ. Spectroscopic characterization of complexes of ruthenium(II) and iridium(III) with 4,4′-diphenyl-2,2′-bipyridine and

4,7-diphenyl-1,10-phenanthroline. Journal of the American Chemical Society 1971;93(13):3184–8.
[38] Karapire C, Timur C, Içli S. A comparative study of the photophysical properties of perylenediimides in liquid phase, PVC and sol–gel host matrices. Dyes and Pigments 2003;56(2):135–43.
[39] Gryczynski I, Kusba J, Lakowicz J. Effects of light quenching on the emission spectra and intensity decays of fluorophore mixtures. Journal of Fluorescence 1997;7(3):167–83.
[40] Chu BW-K, Yam VW-W. Sensitive single-layered oxygen-sensing systems: polypyridyl Ruthenium(II) complexes covalently attached or deposited as Langmuir–Blodgett monolayer on glass surfaces. Langmuir 2006;22(17): 7437–43.
[41] Payra P, Dutta PK. Development of a dissolved oxygen sensor using tris(bipyridyl) ruthenium (II) complexes entrapped in highly siliceous zeolites. Microporous and Mesoporous Materials 2003;64(1–3):109–18.
[42] Yap CC, Yahaya M, Salleh MM. The effect of driving voltage on the electroluminescent property of a blend of poly(9-vinylcarbazole) and 2-(4-biphenylyl)-5-phenyl-1,3,4-oxadiazole. Current Applied Physics 2009; 9(5):1038–41.
[43] Desilets DJ, Kissinger PT, Lytle FE. Improved method for determination of Stern-Volmer quenching constants. Analytical Chemistry 1987;59(8):1244–6.
[44] Kim B-S, Kim S-H, Kim Y-S, Kim S-H, Son Y-A. Synthesis and characterization of quinoline-based dye sensor. Molecular Crystals and Liquid Crystals 2009; 504:173–80.
[45] Chao Y-C, Huang S-Y, Chen C-Y, Chang Y-F, Meng H-F, Yen F-W, et al. Highly efficient solution-processed red organic light-emitting diodes with long-side-chained triplet emitter. Synthetic Metals 2011;161(1–2):148–52.
[46] Sekiguchi Y, Habuchi S, Vacha M. Nanoscale heterogeneity and light-emission dynamics in solution-processed phosphorescent organic light-emitting devices. Physical Chemistry Chemical Physics 2009;11(39):8684–8.
[47] You Y, Kim SH, Jung HK, Park SY. Blue electrophosphorescence from iridium complex covalently bonded to the poly(9-dodecyl-3-vinylcarbazole): suppressed phase segregation and enhanced energy transfer. Macromolecules 2005;39(1):349–56.
[48] Ho CL, Wong WY, Zhou GJ, Yao B, Xie Z, Wang L. Solution-processible multicomponent cyclometalated iridium phosphors for high-efficiency orange-emitting OLEDs and their potential use as white light sources. Advanced Functional Materials 2007;17(15):2925–36.